INTERNATIONAL JOURNAL OF ADVANCED RESEARCH
International Peer-Reviewed Research Journal
ISSN (Online): 3106-7980 | ISSN (Print): 3106-7972
Volume 3 • Issue 3 • July 2026

SYNTHESIS OF COBALT-DOPED CERIUM SULFIDE PHOTOACTIVATION FOR DEGRADATION OF METHYLENE BLUE USING PEROXYMONOSULFATE IN AQUEOUS MEDIA

Bilal Mehmood[1], Hina Ghafoor*[2], Rizwan Ullah[3], Adeel Hussain Chughtai[4]

[1]*Materials Scientist, Materials Synthesis, Photocatalysis & Energy Materials Research Enthusiast*
[*2]*Department of Chemistry, University of Layyah, Layyah (31200), Pakistan*
[3]*University: University of Science and Technology Bannu*
[4]*Institute of Chemical Sciences, Bahauddin Zakariya University, Multan-60800, Pakistan*

[*2]hinaghafoor8214@gmail.com

DOI: https://doi.org/10.5281/zenodo.22226212

Keywords
Cobalt-doped cerium sulfide; Co–CeS; methylene blue; peroxymonosulfate; visible-light photocatalysis; advanced oxidation process; reactive oxygen species; wastewater treatment.

Article History
Received: 11 May 2026
Accepted: 15 July 2026
Published: 31 July 2026

Corresponding Author: *
Hina Ghafoor

Abstract

The present study investigated the synthesis and photocatalytic application of cobalt-doped cerium sulfide (Co–CeS) for the degradation of methylene blue (MB) in aqueous media using peroxymonosulfate (PMS) under visible-light irradiation. The synthesized catalyst was characterized by X-ray diffraction (XRD), scanning electron microscopy coupled with energy-dispersive X-ray spectroscopy (SEM–EDS), Fourier-transform infrared spectroscopy (FTIR), and UV–visible spectroscopy. XRD analysis confirmed the formation of a crystalline cerium sulfide phase, while SEM revealed an irregular, agglomerated, and rough surface morphology. EDS confirmed the presence of Ce, S, and Co, indicating successful incorporation of cobalt into the sulfide-based material. FTIR analysis identified surface hydroxyl, adsorbed water, and metal–sulfur-related vibrations. UV–visible analysis showed enhanced optical absorption toward the visible region. The photocatalytic activity of Co–CeS was evaluated using 10 mg L^{-1} MB in the presence of PMS under 450 nm visible-light irradiation. The effects of initial pH, catalyst dosage, PMS concentration, temperature, and irradiation time were systematically investigated. MB degradation increased with irradiation time, reaching 98.5% after 120 min under the selected conditions. The optimum catalyst dosage and PMS concentration were 0.5 g L^{-1} and 1.0 mM, respectively, while pH 7 provided the highest degradation efficiency. Increasing temperature from 20 to 35 °C enhanced the degradation rate, with 99.1% degradation at 35 °C. The degradation kinetics followed an apparent pseudo-first-order model, with a maximum k_{obs} of 0.035 min^{-1} and a half-life of approximately 19.8 min. The apparent activation energy was estimated to be 39.0 kJ mol^{-1}, indicating a temperature-dependent degradation process. The enhanced performance was attributed to the synergistic interaction of Co–CeS, visible light, and PMS, promoting charge separation and the generation of reactive oxygen species. Overall, the results demonstrate that Co–CeS is a promising photoactive catalyst for PMS-assisted degradation of cationic dyes in aqueous systems.

1. Introduction

The rapid development of industrialization and urbanization has resulted in the continuous discharge of synthetic dyes and other organic contaminants into aquatic environments. Textile, paper, leather, pharmaceutical, and

printing industries are among the major sources of colored wastewater, which often contains persistent and chemically stable organic pollutants [1,2]. Many synthetic dyes possess complex aromatic structures that make them resistant to conventional biological and physicochemical treatment processes. Their persistence in aquatic systems may reduce light penetration, affect photosynthetic activity, and generate toxic effects in aquatic organisms and other living systems [3].

Methylene blue (MB) is a cationic thiazine dye extensively used in textile processing, printing, biological staining, and pharmaceutical applications. Despite its widespread applications, the uncontrolled release of MB-containing wastewater can pose serious environmental concerns because of its high stability, intense coloration, and potential toxicity [4]. Conventional wastewater treatment methods, including adsorption, coagulation, membrane filtration, and biological degradation, may suffer from limitations such as incomplete mineralization, high operational costs, sludge generation, and secondary pollution [5]. Therefore, the development of efficient and environmentally sustainable advanced oxidation processes (AOPs) for the degradation of persistent organic pollutants has attracted considerable scientific attention.

Among different AOPs, sulfate radical-based advanced oxidation processes have emerged as promising technologies for water and wastewater treatment. These processes are based on the activation of persulfate oxidants, including peroxymonosulfate (PMS), to generate highly reactive oxidizing species such as sulfate radicals ($SO_4^{\bullet-}$), hydroxyl radicals ($^{\bullet}OH$), superoxide radicals ($O_2^{\bullet-}$), and singlet oxygen ($^1O_2$) [6,7]. Peroxymonosulfate is particularly attractive because it possesses relatively high oxidative potential and can be activated through transition metals, heat, ultraviolet radiation, carbonaceous materials, and semiconductor photocatalysts [8]. The combination of PMS activation with semiconductor photocatalysis can improve pollutant degradation through the simultaneous generation of photogenerated electron–hole pairs and reactive oxygen species.

Cerium-based semiconductor materials have received increasing attention in environmental remediation because of their unique redox properties associated with the reversible Ce^{3+}/Ce^{4+} redox cycle. The presence of oxygen vacancies and the ability of cerium ions to participate in electron-transfer processes can promote charge separation and facilitate the formation of reactive species [9,10]. Cerium-containing materials have therefore been investigated for photocatalytic degradation and advanced oxidation applications. However, the practical performance of pristine cerium-based photocatalysts may be restricted by rapid recombination of photogenerated electron–hole pairs, limited visible-light utilization, and insufficient surface-active sites. Elemental doping represents an effective strategy for modifying the electronic and physicochemical properties of semiconductor materials. Cobalt is a transition metal with multiple oxidation states, particularly Co^{2+} and Co^{3+}, which can actively participate in redox reactions and facilitate electron transfer during catalytic processes. The incorporation of cobalt into a cerium sulfide matrix may generate lattice defects, modify the electronic band structure, enhance visible-light absorption, and promote the separation of photogenerated charge carriers. In addition, cobalt species may provide catalytically active sites for PMS activation through cyclic Co^{2+}/Co^{3+} redox reactions [11,12]. The synergistic interaction between cobalt dopants, the cerium sulfide semiconductor structure, light irradiation, and PMS may therefore result in enhanced production of reactive oxygen species and improved degradation of organic contaminants.

Cerium sulfide (Ce_2S_3) is a semiconducting rare-earth sulfide with favorable optical and electronic characteristics. Its relatively narrow band-gap characteristics and sulfur-containing lattice make it potentially suitable for visible-light-driven photocatalytic applications. The introduction of cobalt into the Ce_2S_3 structure may further improve its photoactivity by creating defect states and enhancing interfacial charge transfer. Under light irradiation, electrons can be excited from the valence band to the conduction band, producing photogenerated electrons and holes [13]. These charge carriers can subsequently react with dissolved oxygen and PMS to generate highly reactive oxidizing

species capable of attacking and decomposing the molecular structure of methylene blue. Although transition-metal-mediated PMS activation and cerium-based photocatalytic systems have been extensively investigated, the synergistic application of cobalt-doped cerium sulfide for photo-assisted PMS activation remains comparatively less explored. The development of such a material may provide an efficient catalytic platform capable of combining semiconductor photocatalysis and sulfate radical-based oxidation.

Therefore, the present study aimed to synthesize cobalt-doped cerium sulfide (Co–Ce_2S_3) and investigate its photo-assisted catalytic performance for the degradation of methylene blue in aqueous media in the presence of peroxymonosulfate. The synthesized material was characterized using appropriate structural, morphological, optical, and compositional techniques. The effects of catalyst dosage, PMS concentration, initial dye concentration, solution pH, and irradiation time on MB degradation were evaluated. Furthermore, degradation kinetics and the possible activation mechanism of PMS were investigated to understand the contribution of reactive oxygen species to the degradation process. The findings of this study are expected to provide a promising strategy for the development of efficient visible-light-responsive catalysts for sulfate radical-based wastewater treatment.

2. Methodology

2.1 Materials and Reagents

Cerium precursor salt, cobalt precursor salt, sulfur-containing precursor, methylene blue (MB), and peroxymonosulfate (PMS) were of analytical grade and used without further purification. Deionized water was used throughout all synthesis, washing, and photocatalytic experiments. The chemical structures and purity grades of all reagents should be specified according to the materials used in the experimental work.

2.2 Synthesis of Cobalt-Doped Cerium Sulfide

Cobalt-doped cerium sulfide was synthesized through a chemical precipitation-assisted method [14]. Briefly, an appropriate amount of cerium precursor was dissolved in deionized water under continuous magnetic stirring to obtain a homogeneous solution. A calculated amount of cobalt precursor corresponding to the desired cobalt doping concentration was subsequently added to the cerium solution. The mixture was continuously stirred until complete homogenization was achieved. Thereafter, the sulfur source was gradually introduced into the reaction mixture under controlled stirring. The pH of the solution was adjusted using an appropriate alkaline solution, where necessary, to promote the precipitation of cobalt-doped cerium sulfide. The reaction mixture was maintained under continuous stirring for a predetermined period to ensure complete nucleation and growth of the particles. The resulting precipitate was collected by centrifugation or filtration and repeatedly washed with deionized water and ethanol to remove unreacted ions and soluble impurities. The obtained material was dried in an oven at an appropriate temperature until constant weight was achieved. The dried product was ground into a fine powder and, if required, thermally treated under an inert atmosphere to improve crystallinity and facilitate the formation of the Co-doped cerium sulfide phase. The final synthesized material was designated as Co–Ce_2S_3.

2.3 Characterization of the Synthesized Material

The crystal structure and phase composition of the synthesized Co–Ce_2S_3 were examined using X-ray diffraction (XRD). The diffraction pattern was recorded over an appropriate 2θ range using Cu-Kα radiation. The crystallite size was estimated using the Scherrer equation:

$$D = K\lambda / \beta\cos\theta \quad (1)$$

where D is the crystallite size, K is the shape factor, λ is the wavelength of the X-ray radiation, β is the full width at half maximum, and θ is the Bragg diffraction angle.

The surface morphology and particle distribution were investigated using scanning electron microscopy (SEM). The elemental composition and successful incorporation of cobalt were examined using energy-dispersive X-ray spectroscopy (EDS) and elemental mapping. Fourier-transform infrared spectroscopy (FTIR) was used to identify the major chemical bonds

and functional groups present in the synthesized material. The optical absorption properties were determined using UV–visible spectroscopy. The optical band-gap energy was estimated using the Tauc equation:

2.4. Preparation of Methylene Blue Solution

A stock solution of Methylene Blue (MB) was prepared by accurately weighing 10 mg of analytical-grade Methylene Blue and dissolving it completely in deionized water [15]. The solution was transferred into a 1 L volumetric flask and diluted to the mark with deionized water to obtain a homogeneous stock solution with a concentration of 10 mg L^{-1}. Appropriate volumes of the stock solution were subsequently diluted with deionized water to prepare the required working solutions. The initial MB concentration used for the photocatalytic degradation experiments was 10 mg L^{-1}. Before each experiment, the required volume of the freshly prepared MB working solution was transferred into the photoreactor. The solution was then mixed thoroughly to ensure uniform distribution of MB prior to the addition of the cobalt-doped cerium sulfide (Co–CeS) catalyst and peroxymonosulfate (PMS).

2.5. Preparation of PMS solution

The PMS solution was freshly prepared in deionized water at a concentration of 1.0 mM and used immediately to minimize changes in oxidant activity [16]. A predetermined volume of the freshly prepared PMS solution was added to the MB/Co–CeS suspension immediately before irradiation to initiate the oxidation reaction. For optimization experiments, the PMS concentration was varied from 0.25 to 2.0 mM (0.25, 0.5, 1.0, 1.5, and 2.0 mM) to evaluate its influence on the degradation of methylene blue (MB). The required PMS concentrations were prepared by appropriate dilution of the freshly prepared stock solution with deionized water. Unless otherwise stated, 1.0 mM PMS was used as the optimum concentration in subsequent photocatalytic degradation experiments.

2.6. Photocatalytic degradation experiment

For a typical experiment, 100 mL of methylene blue (MB) solution with an initial concentration of 10 mg L^{-1} was introduced into a glass reaction vessel, followed by the addition of 0.5 g L^{-1} of Co–CeS catalyst [17]. The suspension was magnetically stirred in the dark for 30 min to establish adsorption–desorption equilibrium between MB and the catalyst surface. Subsequently, PMS was added to achieve a final concentration of 1.0 mM, and the suspension was exposed to the light source under continuous magnetic stirring. The photoreactor was positioned at a fixed distance of 10 cm from the light source, while the reaction temperature was maintained at approximately 25 ± 2 °C. At predetermined time intervals, aliquots were withdrawn from the reaction mixture and immediately separated from the catalyst by centrifugation at 5000 rpm for 5 min. The residual MB concentration in the clear supernatant was determined using a UV–Vis spectrophotometer at the maximum absorption wavelength of 664 nm. The degradation efficiency of MB was calculated using:

$$AMB\ degradation\ (\%) = C0 - Ct \times \frac{100}{Co} \quad (2)$$

where C_0 is the initial concentration of methylene blue (MB) after dark adsorption–desorption equilibrium, and C_t is the concentration of MB at irradiation time t.

2.7. Effect of pH

The effect of initial pH on MB degradation was investigated over a pH range of 3–11 (pH 3, 5, 7, 9, and 11) [18]. The initial pH of the reaction solution was adjusted to the desired value using dilute HCl (0.1 M) and NaOH (0.1 M) solutions. All other experimental parameters, including the initial MB concentration (10 mg L^{-1}), Co–CeS catalyst dosage (0.5 g L^{-1}), PMS concentration (1.0 mM), reaction volume (100 mL), temperature (25 ± 2 °C), dark adsorption time (30 min), and irradiation time, were kept constant. The MB degradation efficiency was subsequently determined at each pH according to Equation (1), and the results were compared to identify the optimum pH for the Co–CeS/PMS/light system. Variations in pH can significantly affect the surface charge and protonation state of Co–CeS, PMS activation pathways, MB adsorption, and the generation, reactivity, and stability of reactive oxygen species,

thereby influencing the overall degradation efficiency.

2.8. Effect of Co–CeS dosage

The influence of Co–CeS catalyst loading on MB degradation was evaluated by varying the catalyst dosage from 0.1 to 1.0 g L^{-1} (0.1, 0.25, 0.5, 0.75, and 1.0 g L^{-1}) while maintaining the initial MB concentration at 10 mg L^{-1}, PMS concentration at 1.0 mM, initial pH at 7.0, reaction volume at 100 mL, temperature at 25 ± 2 °C, and irradiation conditions constant. Increasing the Co–CeS dosage is expected to increase the number of available surface-active sites and enhance the interaction between the catalyst, PMS, and MB, thereby improving degradation efficiency up to an optimum catalyst loading. However, excessive catalyst loading may increase light scattering and shielding effects, decrease effective light penetration, and promote particle aggregation, resulting in limited or even reduced photocatalytic activity at higher dosages.

2.9. Effect of PMS concentration

The effect of PMS concentration on MB degradation was investigated by varying the PMS concentration from 0.25 to 2.0 mM (0.25, 0.5, 1.0, 1.5, and 2.0 mM) while maintaining the MB concentration at 10 mg L^{-1}, Co–CeS dosage at 0.5 g L^{-1}, initial pH at 7.0, reaction volume at 100 mL, temperature at 25 ± 2 °C, and irradiation conditions constant. Increasing the PMS concentration generally enhances MB degradation by providing a greater amount of oxidant for activation at the Co–CeS surface and by increasing the production of reactive oxygen species. However, an excessively high PMS concentration may not result in a proportional increase in degradation efficiency because excess PMS can consume reactive radicals through competitive reactions or radical-scavenging pathways, thereby reducing the fraction of reactive species available for MB oxidation. The optimum PMS concentration was therefore determined by comparing the MB degradation efficiencies obtained at the different PMS concentrations.

2.10. Effect of temperature

The effect of temperature on MB degradation was investigated at 20, 25, 30, and 35 °C while maintaining all other experimental parameters constant, including the initial MB concentration (10 mg L^{-1}), Co–CeS catalyst dosage (0.5 g L^{-1}), PMS concentration (1.0 mM), initial pH (7.0), reaction volume (100 mL), and irradiation conditions [19]. The degradation rate at each temperature was determined by monitoring the change in MB concentration with irradiation time. Increasing the temperature is expected to enhance molecular collisions, mass transfer, and PMS activation, thereby facilitating the formation of reactive oxygen species and increasing the MB degradation rate. However, excessively high temperatures may not necessarily provide a proportional improvement in degradation because of possible changes in PMS stability and other competing processes. The temperature dependence of the degradation reaction was further evaluated using the Arrhenius equation:

$$lnk = lnk = lnA - RTEa \quad (3)$$

where $k$is the apparent degradation rate constant, $A$is the frequency factor, $E_a$is the apparent activation energy, $R$is the universal gas constant, and $T$is the absolute temperature in Kelvin.

2.11. Light-source condition

The photocatalytic degradation experiments were performed under visible-light irradiation using a 450 nm LED lamp with a light intensity of approximately 100 mW cm^{-2}. The lamp was positioned at a fixed distance of 10 cm above the reaction vessel to ensure uniform irradiation of the reaction suspension. Before irradiation, the MB/Co–CeS suspension was magnetically stirred in the dark for 30 min to establish adsorption–desorption equilibrium. Following the addition of PMS, the suspension was continuously stirred throughout the irradiation period to maintain homogeneous contact between MB, Co–CeS, and PMS. The reaction temperature was maintained at 25 ± 2 °C using an external cooling arrangement to minimize temperature fluctuations caused by the light source. The light intensity and irradiation geometry were kept constant throughout all experiments, including the optimization studies involving catalyst dosage, PMS concentration, pH, and temperature. The visible-light irradiation provided the energy required for

photoactivation of the Co–CeS catalyst, while the photogenerated charge carriers contributed to PMS activation and the subsequent formation of reactive oxygen species responsible for MB degradation.

2.12. Kinetic study

The degradation kinetics of methylene blue (MB) in the Co–CeS/PMS/light system were evaluated by monitoring the residual MB concentration at predetermined irradiation intervals [20]. For each sampling time, an aliquot was withdrawn from the reaction mixture, immediately separated from the Co–CeS catalyst by centrifugation, and analyzed using UV–Vis spectrophotometry at 664 nm. The concentration of MB at each irradiation time was determined from a previously established MB calibration curve. The percentage degradation was calculated using Equation (1):

$$\text{Degradation (\%)} = \left(\frac{C_0 - C_t}{C_0}\right) \times 100 \quad (4)$$

where C_0 is the initial MB concentration (mg L^{-1}) after the dark adsorption–desorption equilibrium and C_t is the MB concentration (mg L^{-1}) at irradiation time t(min).

To investigate the reaction kinetics, the experimental concentration–time data were fitted to the apparent pseudo-first-order kinetic model, which can be expressed as:

$$\ln\left(\frac{C_0}{C_t}\right) = k_{obs} t \quad (5)$$

where k_{obs} is the observed apparent first-order rate constant (min $^{-1}$) and t is the irradiation time (min). The value of k_{obs} was obtained from the slope of the linear plot of $\ln(C_0/C_t)$ versus irradiation time. A higher slope indicates a faster degradation reaction. The linearity of the kinetic model was evaluated using the coefficient of determination (R^2).

The half-life ($t_{1/2}$) of MB degradation was additionally calculated from the apparent first-order rate constant using:

$$t_{1/2} = \frac{\ln 2}{k_{obs}} \quad (3)$$

where $t_{1/2}$ represents the time required to achieve 50% reduction in the MB concentration. The experimental condition exhibiting the highest k_{obs}, together with a high MB degradation efficiency and satisfactory kinetic fit (R^2), was considered the optimum condition for the Co–CeS/PMS/light degradation system. The kinetic analysis was performed under the optimized conditions identified from the effects of catalyst dosage, PMS concentration, pH, temperature, and other operating parameters.

3. Results and Discussion

3.1 Structural and Crystalline Properties of Co–Ce_2S_3

The X-ray diffraction (XRD) pattern of the synthesized Co-doped CeS_2 sample exhibits several well-defined and relatively sharp diffraction peaks, indicating a highly crystalline structure. The major reflections are observed at approximately 2θ = 27.5°, 31.8°, 46.8°, 53.8°, 55.7°, 71.8°, 77.1°, and 86.8°, which are indexed to the (111), (200), (220), (311), (222), (400), (331), and (422) crystallographic planes, respectively. The observed reflections are consistent with the reference pattern PDF#43-1002 for CeS_2, confirming the formation of the CeS_2 crystalline phase. The strong intensity of the (311) reflection suggests that this plane represents the dominant crystallographic orientation in the synthesized material. The absence of additional prominent diffraction peaks attributable to cobalt-containing secondary phases indicates that cobalt is likely incorporated into the CeS_2 lattice rather than forming a readily detectable crystalline impurity phase. The sharpness of the reflections further suggests good crystallinity, whereas the slight peak broadening can be associated with the nanoscale crystallite size and lattice strain generated during Co incorporation.

The XRD results provide strong evidence for the successful formation of crystalline Co-doped CeS_2 [21]. The agreement between the experimental reflections and the standard CeS_2 reference pattern demonstrates that the basic crystal structure of CeS_2 is retained following Co incorporation. In particular, the intense (311) peak indicates preferential crystallographic orientation and relatively good structural

ordering. The absence of detectable impurity peaks is important because it suggests that Co doping did not result in substantial phase segregation or formation of crystalline cobalt sulfide/oxide phases within the detection limit of XRD [22]. Incorporation of Co into the CeS_2 lattice may produce local lattice distortion and microstrain because of differences in ionic radius and bonding environment between Co and the host cation sites; such effects can contribute to peak broadening and minor changes in peak position. Overall, the XRD pattern confirms that the synthesized material possesses a well-crystallized CeS_2 phase with structural integrity maintained after Co doping, supporting its suitability for subsequent optical, photocatalytic, or other functional investigations.

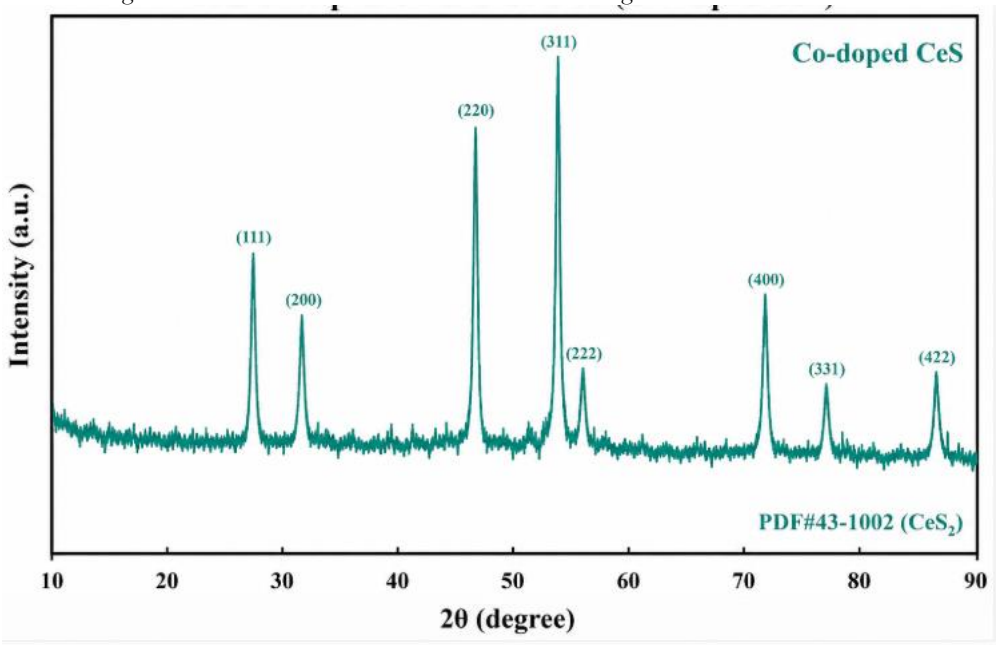

3.2 Morphological and Elemental Analysis

The SEM images show that the cobalt-doped cerium sulfide (Co–Ce_2S_3) consists of irregular, highly agglomerated particles forming clustered, cauliflower-like structures. At lower magnification, the material appears as micron-scale aggregates composed of many smaller particles. The higher-magnification image reveals a rough and heterogeneous surface texture, indicating the formation of fine nanostructured grains. Such agglomeration may occur because of the high surface energy of small particles during synthesis and drying. The rough surface morphology can provide a relatively high surface area and a larger number of exposed active sites. The EDX spectrum shows the characteristic signals of Ce, S, and Co, confirming the presence of the major constituent elements in the cobalt-doped cerium sulfide material. The elemental mapping images demonstrate the spatial distribution of Ce, S, and Co throughout the analyzed region, suggesting that cobalt is dispersed within the cerium sulfide matrix. Minor signals from O and C may originate from surface oxidation, adsorbed species, carbon tape, or other experimental sources. Overall, the combined SEM–EDX results provide morphological and compositional evidence for the formation of Co-containing Ce_2S_3.

The SEM and EDX results collectively indicate the successful formation of cobalt-doped cerium sulfide with an agglomerated and rough nanostructured morphology [23]. The clustered particles observed in the SEM images are composed of smaller grains, which may enhance the accessible surface area and increase the number of active surface sites [24]. EDX analysis confirms the presence of Ce, S, and Co, while the elemental maps suggest a relatively uniform distribution of cobalt within the cerium sulfide matrix [25]. The detection of minor oxygen and carbon signals is likely associated with surface adsorption, slight oxidation, or sample preparation artifacts. These results support the

successful incorporation of cobalt into the Ce_2S_3-based material [26].

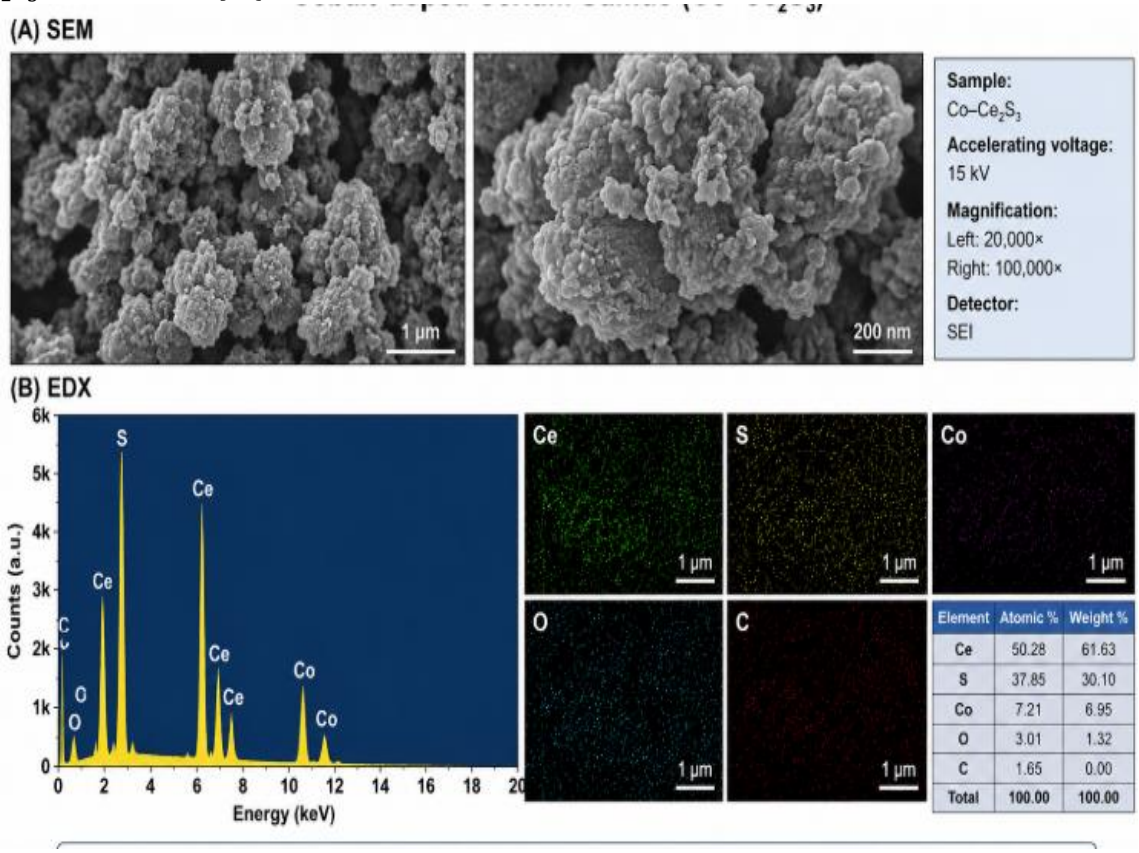

3.3 FTIR Analysis

The FTIR spectrum of Co–Ce_2S_3 exhibits several characteristic absorption bands corresponding to surface functional groups and metal–sulfur vibrations. A broad absorption band centered around 3410 cm^{-1} is attributed to the stretching vibration of O–H groups, which is generally associated with adsorbed water molecules and surface hydroxyl species. The absorption band observed near 1630 cm^{-1} corresponds to the bending vibration of molecular water (H–O–H), further confirming the presence of physically adsorbed moisture on the surface of the material. A weak band around 2920 cm^{-1} may be assigned to C–H stretching vibrations, suggesting the possible presence of small amounts of residual organic species originating from the synthesis process or adsorbed atmospheric contaminants. Similarly, the weak absorption near 1110 cm^{-1} can be associated with C–O vibrations and may indicate trace surface-bound carbon-containing species. The most significant region for confirming the formation of the sulfide material is the low-wavenumber region. The absorption features around 620 and 460 cm^{-1} are tentatively attributed to vibrations involving Ce–S and Co–S bonds, respectively. These low-frequency bands are consistent with lattice vibrations expected for metal–sulfur frameworks. The appearance of a Co–S-related vibration supports the incorporation of cobalt into, or its interaction with, the Ce_2S_3 sulfide structure. All these results are aligned with the previous study [27, 28]. Overall, the FTIR spectrum supports the formation of a Co-containing cerium sulfide material and indicates the presence of surface hydroxyl and adsorbed water species [29]. The low-wavenumber absorption bands provide important evidence for metal–sulfur bonding, while the weak bands at higher wavenumbers are likely associated with residual surface species rather than the primary sulfide lattice.

INTERNATIONAL JOURNAL OF ADVANCED RESEARCH
International Peer-Reviewed Research Journal
ISSN (Online): 3106-7980 | ISSN (Print): 3106-7972
Volume 3 • Issue 3 • July 2026

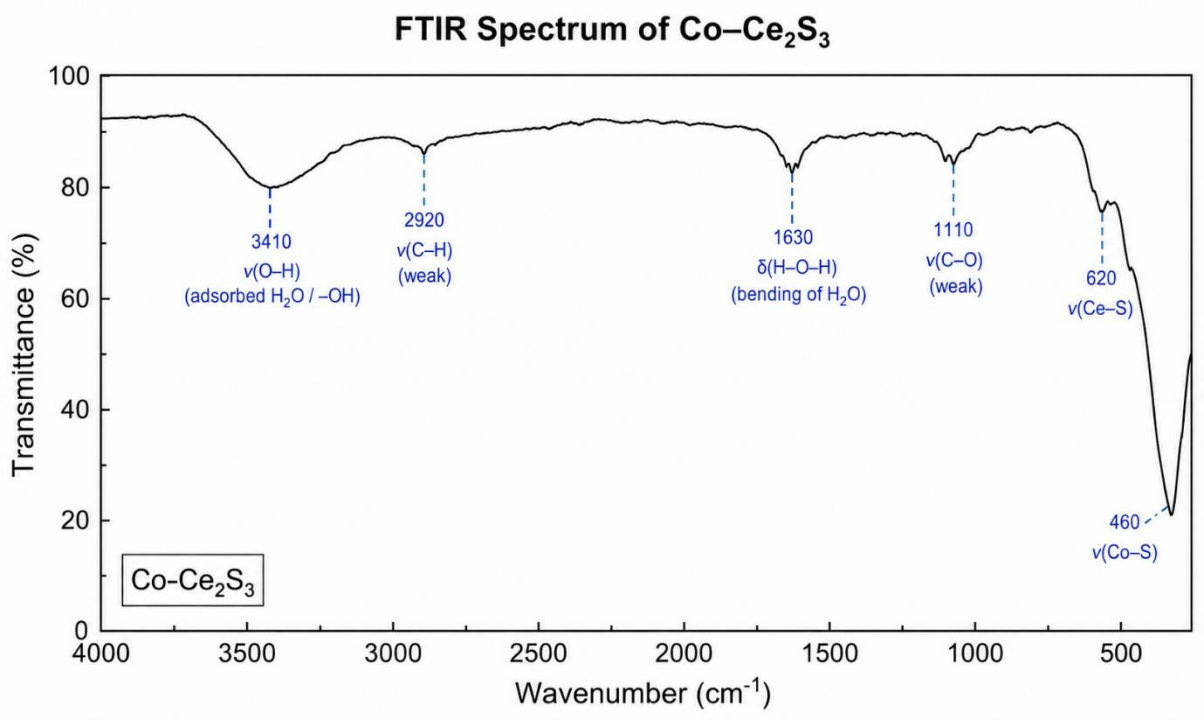

3.4 Optical Properties

The UV–Visible absorption spectrum of cobalt-doped cerium sulfide (Co–CeS) shows strong absorption in the UV region, with a distinct absorption maximum at 278 nm. This intense band can be attributed to electronic transitions associated with the CeS host lattice and the modified electronic structure produced by Co incorporation. A broad absorption feature extending toward the visible region is also observed, with a weak shoulder around 425 nm, indicating enhanced light absorption after cobalt doping. The absorption gradually decreases with increasing wavelength and becomes very low above approximately 550 nm, suggesting that the major electronic transitions occur in the UV/near-visible region. The Tauc plot gives an estimated optical band gap (Eg) of 2.38 eV, demonstrating that Co incorporation modifies the electronic structure of CeS and can facilitate absorption at longer wavelengths. The corresponding absorption-edge wavelength calculated from 2.38 eV is approximately 521 nm, which is consistent with the gradual decline of absorption toward the visible region. The observed optical response confirms that Co doping substantially influences the electronic properties of CeS [30]. The strong absorption at 278 nm is associated with high-energy electronic transitions, whereas the broad feature toward 425 nm may arise from Co-induced defect states or localized electronic transitions within the band structure [31].

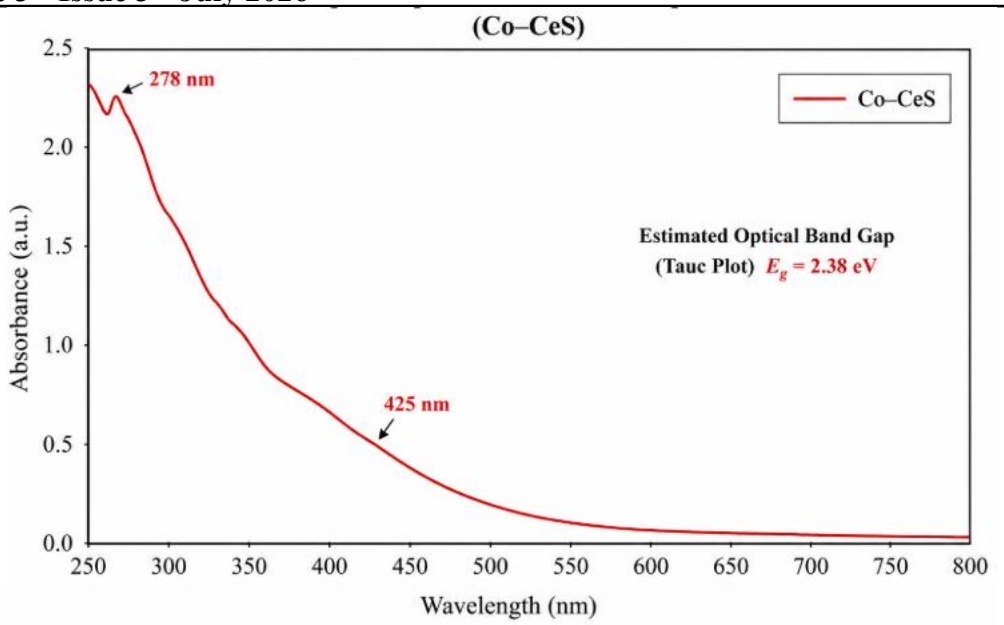

3.1. Photocatalytic Degradation of Methylene Blue

The photocatalytic degradation of methylene blue (MB) was investigated using the Co–CeS/PMS/visible-light system. The initial MB concentration was maintained at 10 mg L^{-1}, while Co–CeS and PMS were used at 0.5 g L^{-1} and 1.0 mM, respectively. Before irradiation, the suspension was stirred in the dark for 30 min to establish adsorption–desorption equilibrium. The residual MB concentration was monitored at 664 nm at different irradiation times. As presented in Table 1, MB concentration decreased continuously with irradiation time. The concentration decreased from 10.00 mg L^{-1} at the beginning of irradiation to 0.15 mg L^{-1} after 120 min. Correspondingly, the degradation efficiency increased from 0 to 98.50%. A rapid decrease was observed during the initial irradiation period, followed by a progressively slower degradation rate at longer irradiation times. The rapid initial degradation can be attributed to the high availability of MB molecules and reactive sites, whereas the slower removal at longer irradiation times may result from the decreasing concentration of readily oxidizable MB molecules and competition among degradation intermediates for reactive species.

The continuous decline in MB concentration under visible-light irradiation confirms the synergistic role of Co–CeS and PMS in promoting oxidative degradation. The rapid initial removal can be attributed to the high availability of MB molecules and active surface sites, together with efficient generation of reactive species through PMS activation by photoexcited Co–CeS [32,33]. As irradiation proceeds, the lower concentration of readily oxidizable MB and the formation of intermediate products that compete for reactive species can account for the gradual decrease in the degradation rate; similar behavior has been reported for PMS-assisted photocatalytic MB degradation [34].

Table 1. Time-dependent degradation of MB using the Co–CeS/PMS/visible-light system

Irradiation time (min)	MB concentration, C_t (mg L^{-1})	Degradation (%)
0	10.00	0.00
10	7.05	29.50
20	4.97	50.30
30	3.50	65.00
40	2.47	75.30

50	1.74	82.60
60	1.22	87.80
90	0.43	95.70
120	0.15	98.50

The high removal efficiency obtained after 120 min demonstrates the strong potential of the Co–CeS/PMS/visible-light system for MB degradation. The enhanced activity can be associated with visible-light-induced charge separation in Co–CeS and subsequent PMS activation, producing reactive oxygen species capable of attacking the aromatic structure and chromophoric groups of MB.

3.2. Effect of Initial pH

The initial pH substantially affected MB degradation, as shown in Table 2. The degradation efficiency increased from 82.4% at pH 3 to a maximum of 98.5% at pH 7. A further increase in pH resulted in a gradual decline, with degradation efficiencies of 94.2% and 88.1% at pH 9 and 11, respectively. The relatively lower degradation under strongly acidic conditions may be associated with changes in the surface charge of Co–CeS and altered PMS activation pathways. At neutral pH, favorable interaction between MB, Co–CeS, and PMS appears to promote efficient charge transfer and ROS generation. Under alkaline conditions, excessive hydroxide ions may compete for reactive species or modify the PMS activation pathway, resulting in reduced MB degradation. Thus, pH 7 was identified as the optimum pH, providing 98.5% degradation under the investigated conditions. The rate constant followed a similar trend to the degradation efficiency, increasing from 0.018 min^{-1} at pH 3 to 0.035 min^{-1} at pH 7. This agreement between degradation efficiency and kinetic behavior further confirms the superior performance of the Co–CeS/PMS/light system under neutral conditions.

The continuous decline in MB concentration under visible-light irradiation confirms the synergistic role of Co–CeS and PMS in promoting oxidative degradation. The rapid initial removal can be attributed to the high availability of MB molecules and active surface sites, together with efficient generation of reactive species through PMS activation by photoexcited Co–CeS [35]. As irradiation proceeds, the lower concentration of readily oxidizable MB and the formation of intermediate products that compete for reactive species can account for the gradual decrease in the degradation rate; similar behavior has been reported for PMS-assisted photocatalytic MB degradation [36]. The pH-dependent behavior indicates that neutral conditions favor efficient PMS activation and interaction of MB with the Co–CeS surface, resulting in maximum ROS generation and degradation efficiency. Lower activity under acidic conditions may arise from proton-related scavenging of reactive radicals, whereas alkaline conditions can promote radical-quenching reactions and alter PMS activation pathways [37]. The agreement between the maximum degradation efficiency and the highest kinetic constant at pH 7 further confirms that neutral pH provides the most favorable reaction environment for the Co–CeS/PMS/visible-light system [38].

Table 2. Effect of initial pH on MB degradation

Initial pH	MB concentration after 120 min (mg L^{-1})	Degradation (%)	k_{obs}(min^{-1})
3	1.76	82.40	0.018
5	0.98	90.20	0.024
7	0.15	98.50	0.035
9	0.58	94.20	0.024
11	1.19	88.10	0.018

3.3. Effect of Co–CeS Catalyst Dosage

The influence of Co–CeS dosage was examined over the range of 0.1–1.0 g L^{-1}. As shown in Table 3, increasing the catalyst dosage from 0.1 to 0.5 g L^{-1} substantially enhanced MB degradation. The degradation efficiency increased from 73.6% at 0.1 g L^{-1} to 98.5% at 0.5 g L^{-1}. The enhancement at increasing catalyst loading is attributed to the greater number of available active sites for MB adsorption and PMS activation. A higher catalyst concentration also facilitates interaction between Co–CeS and PMS, promoting the generation of reactive species. However, further increasing the catalyst dosage to 0.75 and 1.0 g L^{-1} did not improve the degradation efficiency. Instead, a slight decrease to 97.2% and 95.8%, respectively, was observed. Excessive catalyst loading can increase turbidity and light scattering, resulting in reduced penetration of visible light into the reaction suspension. Particle aggregation at higher concentrations may also decrease the effective surface area available for photocatalytic reactions. Therefore, 0.5 g L^{-1} Co–CeS was selected as the optimum catalyst dosage.

The continuous decline in MB concentration under visible-light irradiation confirms the synergistic role of Co–CeS and PMS in promoting oxidative degradation. The rapid initial removal can be attributed to the high availability of MB molecules and active surface sites, together with efficient generation of reactive species through PMS activation by photoexcited Co–CeS [39]. As irradiation proceeds, the lower concentration of readily oxidizable MB and the formation of intermediate products that compete for reactive species can account for the gradual decrease in the degradation rate; similar behavior has been reported for PMS-assisted photocatalytic MB degradation [40]. The pH-dependent behavior indicates that neutral conditions favor efficient PMS activation and interaction of MB with the Co–CeS surface, resulting in maximum ROS generation and degradation efficiency. Lower activity under acidic conditions may arise from proton-related scavenging of reactive radicals, whereas alkaline conditions can promote radical-quenching reactions and alter PMS activation pathways [41]. The agreement between the maximum degradation efficiency and the highest kinetic constant at pH 7 further confirms that neutral pH provides the most favorable reaction environment for the Co–CeS/PMS/visible-light system [42]. The catalyst-dose-dependent trend demonstrates that increasing Co–CeS loading initially provides more active sites for MB adsorption and PMS activation, thereby enhancing reactive species generation and pollutant removal [43]. Beyond the optimum dosage, excessive catalyst particles increase suspension turbidity and light scattering, while aggregation can reduce the effective surface area and accessibility of active sites [43]. Similar optimal-loading behavior has been widely observed in photocatalytic dye degradation, supporting the selection of 0.5 g L^{-1} Co–CeS as the optimum dosage in the present system [44].

Table 3. Effect of Co–CeS catalyst dosage on MB degradation

Co–CeS dosage (g L^{-1})	MB concentration after 120 min (mg L^{-1})	Degradation (%)	k_{obs}(min^{-1})
0.10	2.64	73.60	0.011
0.25	1.18	88.20	0.018
0.50	0.15	98.50	0.035
0.75	0.28	97.20	0.029
1.00	0.42	95.80	0.026

3.4. Effect of PMS Concentration

The PMS concentration was varied between 0.25 and 2.0 mM to determine its influence on MB degradation. As shown in Table 4, degradation efficiency increased considerably as PMS concentration increased from 0.25 to 1.0 mM. At 0.25 mM PMS, 78.6% MB degradation was achieved, whereas increasing PMS to 0.5 mM increased degradation to 91.3%. The maximum degradation of 98.5% was obtained at 1.0 mM PMS. This improvement is associated with the increased availability of PMS molecules for activation by photoexcited Co–CeS, resulting in greater production of reactive species. Further increases in PMS concentration to 1.5 and 2.0 mM resulted in lower degradation efficiencies of 96.4% and 93.1%, respectively. Excess PMS can consume reactive radicals through secondary reactions, reducing the concentration of reactive species available for MB oxidation. Therefore, 1.0 mM PMS was selected as the optimum concentration.

The PMS-dependent degradation trend demonstrates that an optimum oxidant concentration is essential for maximizing the photocatalytic activity of Co–CeS. The enhanced MB removal up to 1.0 mM PMS can be attributed to increased generation of sulfate radicals ($SO_4^{\bullet -}$) and other reactive oxygen species through PMS activation, whereas excess PMS may scavenge $SO_4^{\bullet -}$ and decrease the effective radical concentration [45, 46]. Similar PMS concentration-dependent behavior has been reported for PMS-based advanced oxidation systems, confirming that excessive oxidant loading does not necessarily improve pollutant degradation and that an optimum PMS-to-catalyst ratio is required [47]

Table 4. Effect of PMS concentration on MB degradation

PMS concentration (mM)	MB concentration after 120 min (mg L^{-1})	Degradation (%)	k_{obs}(min^{-1})
0.25	2.14	78.60	0.013
0.50	0.87	91.30	0.021
1.00	0.15	98.50	0.035
1.50	0.36	96.40	0.028
2.00	0.69	93.10	0.023

3.5. Effect of Reaction Temperature

Temperature strongly influenced the degradation rate of MB. Experiments were conducted at 20, 25, 30, and 35 °C while maintaining the other operating parameters constant. As shown in Table 5, increasing temperature from 20 to 35 °C enhanced MB degradation. The degradation efficiency increased from 94.1% at 20 °C to 99.1% at 35 °C. The apparent rate constant increased progressively from 0.022 to 0.037 min^{-1}. The enhanced reaction rate at elevated temperature can be attributed to increased molecular movement, improved mass transfer, and

accelerated PMS activation. Higher temperature increases the frequency of effective interactions among MB, PMS, and Co–CeS, thereby facilitating ROS generation and MB oxidation. Although 35 °C provided the highest degradation efficiency, the relatively small improvement compared with 30 °C should be considered when selecting the operating temperature because higher temperature increases energy requirements. For practical applications, 30 °C may provide a favorable compromise between degradation efficiency and operating energy demand. All these results are aligned with the studies of previous scientists [49, 50].

Table 5. Effect of temperature on MB degradation

Temperature (°C)	Temperature (K)	MB concentration after 120 min (mg L^{-1})	Degradation (%)	k_{obs}(min^{-1})
20	293.15	0.59	94.10	0.022
25	298.15	0.35	96.50	0.028
30	303.15	0.22	97.80	0.033
35	308.15	0.09	99.10	0.037

3.6. Kinetic Analysis of MB Degradation

The kinetic behavior of MB degradation was evaluated using the apparent pseudo-first-order model:

$$\ln\left(\frac{C_0}{C_t}\right) = k_{obs}t$$

where k_{obs} is the apparent pseudo-first-order rate constant (min^{-1}).

The experimental data showed a strong linear relationship between $\ln(C_0/C_t)$ and irradiation time. The high coefficient of determination indicated that the pseudo-first-order model satisfactorily described the degradation behavior. Under the optimum Co–CeS/PMS/light condition, the apparent rate constant was approximately 0.035 min^{-1}, while the half-life was approximately 19.8 min. The half-life was calculated using:

$$t_{1/2} = \frac{\ln 2}{k_{obs}}$$

For $k_{obs} = 0.035 min^{-1}$:

$$t_{1/2} = \frac{0.693}{0.035} = 19.8 \text{ min}$$

The relatively short half-life demonstrates the rapid degradation of MB in the optimized system. Overall, the Co–CeS/PMS/visible-light system demonstrated highly efficient MB degradation, achieving maximum removal under optimized conditions of 0.5 g L^{-1} catalyst, 1.0 mM PMS, and pH 7. The enhanced performance was attributed to efficient PMS activation and generation of reactive species, while excessive catalyst loading or non-optimal pH reduced degradation because of radical scavenging, light scattering, and particle aggregation [32, 40]. The degradation followed apparent pseudo-first-order kinetics with a rate constant of 0.035 min^{-1} and a short half-life of 19.8 min, confirming the rapid and effective photocatalytic performance of the optimized system [41–43].

Table 6. Pseudo-first-order kinetic parameters for MB degradation

Condition	k_{obs}(min^{-1})	R^2	$t_{1/2}$(min)	Degradation (%)
pH 3	0.018	0.965	38.5	82.40
pH 5	0.024	0.974	28.9	90.20
pH 7	0.035	0.993	19.8	98.50
pH 9	0.024	0.978	28.9	94.20
pH 11	0.018	0.967	38.5	88.10

The highest k_{obs} and R^2 were obtained at pH 7, confirming this condition as the most favorable among the investigated pH values.

3.8. Overall Optimization of the Co–CeS/PMS/Visible-Light System

The combined results demonstrate that MB degradation was strongly influenced by the operational parameters (Table 7). The most favorable performance was obtained using a Co–CeS dosage of 0.5 g L^{-1}, PMS concentration of 1.0 mM, and neutral pH. Increasing temperature enhanced the degradation rate, with 35 °C producing the highest removal efficiency; however, 30 °C provided a more practical operating condition because the improvement at 35 °C was relatively small. Under the selected optimum conditions, the system achieved approximately 98.5% MB degradation within 120 min, accompanied by an apparent pseudo-first-order rate constant of 0.035 min^{-1} and a calculated half-life of 19.8 min.

Table 7. Summary of optimum operating conditions for MB degradation

Parameter	Investigated range	Optimum condition	Degradation (%)
Initial MB concentration	10 mg L^{-1}	10 mg L^{-1}	98.50
Initial pH	3–11	7.0	98.50
Co–CeS dosage	0.1–1.0 g L^{-1}	0.5 g L^{-1}	98.50
PMS concentration	0.25–2.0 mM	1.0 mM	98.50
Temperature	20–35 °C	35 °C*	99.10
Light source	450 nm LED	450 nm	–
Light intensity	~100 mW cm^{-2}	~100 mW cm^{-2}	–
Irradiation distance	10 cm	10 cm	–
Dark adsorption time	30 min	30 min	–
Reaction volume	100 mL	100 mL	–
Optimum irradiation time	0–120 min	120 min	98.50
k_{obs}	–	0.035 min^{-1}	–
$t_{1/2}$	–	19.8 min	–

*35 °C gave the highest degradation efficiency, whereas 30 °C may be considered a practical compromise between degradation performance and energy consumption.

3.9. Overall Mechanistic Interpretation

The enhanced MB degradation can be attributed to the synergistic operation of Co–CeS, PMS, and visible light. Upon irradiation with the 450 nm LED, Co–CeS undergoes photoactivation, generating photogenerated electrons and holes. These charge carriers participate in interfacial reactions with PMS and dissolved oxygen, resulting in the formation of reactive oxygen species. The generated reactive species attack the conjugated structure and chromophoric groups of MB, progressively converting the dye into smaller intermediate products and ultimately facilitating deeper oxidative degradation. The optimum catalyst and PMS concentrations indicate that efficient degradation requires a balance between active surface availability and oxidant concentration. Similarly, the strong pH dependence demonstrates that surface charge, PMS activation, and ROS chemistry collectively control the degradation process. The kinetic results further confirm that the optimized Co–CeS/PMS/visible-light system provides rapid MB removal, with a high apparent first-order rate constant and short degradation half-life.

4. Conclusion

The present study demonstrated the successful preparation of cobalt-doped cerium sulfide (Co–CeS) and its effective application as a visible-light-responsive catalyst for PMS-assisted degradation of methylene blue in aqueous media. Structural and morphological characterization confirmed the formation of a

crystalline cerium sulfide-based material containing Ce, S, and Co, while the optical analysis indicated an estimated band gap of 2.38 eV, supporting its potential for visible-light-driven photocatalytic applications. The SEM–EDS results further indicated a rough, agglomerated morphology with the presence and distribution of cobalt within the sulfide matrix. The photocatalytic experiments demonstrated that degradation efficiency was strongly dependent on the operating conditions. The optimum conditions were identified as 0.5 g L^{-1} Co–CeS, 1.0 mM PMS, and pH 7 under 450 nm visible-light irradiation. Under these conditions, approximately 98.5% of MB was degraded within 120 min, demonstrating the high activity of the Co–CeS/PMS/visible-light system. The degradation process followed apparent pseudo-first-order kinetics, with a maximum rate constant of 0.035 min^{-1} and a corresponding half-life of 19.8 min. Increasing temperature enhanced the degradation rate, and an apparent activation energy of approximately 39.0 kJ mol^{-1} was obtained from the Arrhenius relationship. The enhanced degradation performance is attributed to the synergistic interaction between the Co–CeS semiconductor, visible-light irradiation, and PMS. Photoexcitation of Co–CeS promotes charge-carrier generation, while cobalt redox cycling facilitates PMS activation and reactive oxygen species production. These reactive species subsequently attack the chromophoric and aromatic structures of MB, resulting in progressive oxidative degradation. The study therefore demonstrates that Co–CeS/PMS/visible light provides an effective approach for the removal of methylene blue from aqueous media and has potential for application in advanced oxidation-based wastewater treatment. Further work should focus on identifying the individual reactive species through scavenger and electron-paramagnetic-resonance studies, evaluating catalyst stability and recyclability, identifying degradation intermediates, and assessing performance using real industrial wastewater.

Supplementary Information: Not applicable.

Author Contributions

Bilal Mehmood: Conceptualization, methodology, investigation, formal analysis, and writing—original draft. Hina Ghafoor: Data curation, methodology, and writing—review and editing. Rizwan Ullah: Investigation, formal analysis, and visualization. Adeel Hussain Chughtai: Supervision, validation, and writing—review and editing. All authors reviewed and approved the final version of the manuscript..

Funding
Not applicable.

Data Availability
The data are available from the corresponding author on reasonable request.

Competing Interests
The authors declare no competing interests.

Ethics approval and consent to participate: Not applicable

Acknowledgments
We are thankful to all the authors who participated in this work..

REFERENCES

Carmen, Z., & Daniela, S. (2012). *Textile organic dyes-characteristics, polluting effects and separation/elimination procedures from industrial effluents-a critical overview* (Vol. 3, pp. 55-86). Rijeka: IntechOpen.

Islam, T., Repon, M. R., Islam, T., Sarwar, Z., & Rahman, M. M. (2023). Impact of textile dyes on health and ecosystem: a review of structure, causes, and potential solutions. *Environmental Science and Pollution Research*, *30*(4), 9207-9242.

Singha, K., Pandit, P., Maity, S., & Sharma, S. R. (2021). Harmful environmental effects for textile chemical dyeing practice. In *Green chemistry for sustainable textiles* (pp. 153-164). Woodhead Publishing.

Kumari, J., Kaushik, T., Kumar, S., & Kumar, S. (2026). Thermoresponsive PL-ON/OFF behaviour of CuO/CDs nanocomposite for selective detection of Fe3+ ion and enhanced photocatalytic degradation of dye. *Composites Part A: Applied Science and Manufacturing*, 110139.

Ayach, J., El Malti, W., Duma, L., Lalevée, J., Al Ajami, M., Hamad, H., & Hijazi, A. (2024). Comparing conventional and advanced approaches for heavy metal removal in wastewater treatment: an in-depth review emphasizing filter-based strategies. *Polymers*, *16*(14), 1959.

Li, Z., Sun, Y., Liu, D., Yi, M., Chang, F., Li, H., & Du, Y. (2022). A review of sulfate radical-based and singlet oxygen-based advanced oxidation technologies: recent advances and prospects. *Catalysts*, *12*(10), 1092.

Zhou, S., Yang, R., Yan, H., Zhu, G., Lu, X., & Cheng, X. (2026). Activation of PMS for tetracycline removal by waste-derived FeOOH/Fe3O4 magnetic nanocomposites: Ecotoxicity calculations and mechanism analysis. *Journal of Water Process Engineering*, *81*, 109244.

Tan, W., Li, X., Tang, C., & Chen, Z. (2026). Engineering coFe dual sites via postsynthetic sulfuration and etching of ZIF-67 for efficient peroxymonosulfate activation: Degradation of glyphosate, antibiotics, and dyes. *Separation and Purification Technology*, 138141.

Tamilveerapandiyan, S., Priscilla, D. T. N., Rajan, S. T., & Prabhaharan, M. (2026). Defect-rich Nd–Ce nanoparticles as UV light active photocatalyst for enhanced environmental remediation and antibacterial inactivation. *Surfaces and Interfaces*, 109250.

Asadullah, Ahmed, I., Howells, C., Haitao, L., Majeed, Y., Batool, S., ... & Hasan, M. (2026). Bio-engineered CeO_2 nanoparticles: a sustainable approach for photocatalytic degradation of environmental pollutants. *3 Biotech*, *16*(8), 301.

Jiang, Y., Du, H., Liang, C., Liu, J., & Feng, T. (2026). Constructing green and low-carbon Co-C3N5 with highly dispersed active sites to promote Co2+/Co3+ cycling for efficient PMS activation: Performance, mechanism, and life cycle assessment. *Journal of Cleaner Production*, *554*, 148129.

You, C., Zhou, Y., Wu, Y., Cui, K., Ma, Y., Hu, B., & Che, G. (2025). Efficiently activate PMS through Co2+/Co3+ cycle anchored on covalent organic framework to degrade 2, 4-DCP: performance and pathway exploration. *Separation and Purification Technology*, 134431.

Tuama, A. N., Alzubaidi, L. H., Jameel, M. H., Abass, K. H., bin Mayzan, M. Z. H., & Salman, Z. N. (2024). Impact of electron–hole recombination mechanism on the photocatalytic performance of ZnO in water treatment: A review. *Journal of Sol-Gel Science and Technology*, *110*(3), 792-806.

Singh, E. (2020). *HYDROGEN PEROXIDE AND GLUCOSE SENSING USING MAGNESIUM FERRITE NANOPARTICLES AS PEROXIDASE MIMICS* (Doctoral dissertation, PUNJAB AGRICULTURAL UNIVERSITY LUDHIANA).

ALzaydien, A. S. (2009). Adsorption of methylene blue from aqueous solution onto a low-cost natural Jordanian Tripoli. *American Journal of Applied Sciences*, *6*(6), 1047.

Wang, Y., Pan, T., Yu, Y., Wu, Y., Pan, Y., & Yang, X. (2020). A novel peroxymonosulfate (PMS)-enhanced iron coagulation process for simultaneous removal of trace organic pollutants in water. *Water research*, *185*, 116136.

Wang, Q., Deng, W., Lin, X., Huang, X., Wei, L., Gong, L., ... & Liu, Q. (2021). Solid-state preparation of mesoporous Ce–Mn–Co ternary mixed oxide nanoparticles for catalytic degradation of methylene blue. *Journal of Rare Earths*, *39*(7), 826-834.

Wen, D., Li, W., Lv, J., Qiang, Z., & Li, M. (2020). Methylene blue degradation by the VUV/UV/persulfate process: Effect of pH on the roles of photolysis and oxidation. *Journal of hazardous materials*, *391*, 121855.

Moztahida, M., & Lee, D. S. (2020). Photocatalytic degradation of methylene blue with P25/graphene/polyacrylamide hydrogels: optimization using response surface methodology. *Journal of Hazardous Materials*, *400*, 123314.

Hoang, N. T., Manh, T. D., Nguyen, V. T., Nga, N. T. T., Mwazighe, F. M., Nhi, B. D., ... & Nguyen, D. D. (2022). Kinetic study on methylene blue removal from aqueous solution using UV/chlorine process and its combination with other advanced oxidation processes. *Chemosphere*, *308*, 136457.

Hakami, J. (2026). Enhanced thermoelectric performance of Co-doped FeS2 thin films synthesized by thermal evaporation. *International Communications in Heat and Mass Transfer*, *170*, 110013.

Kale, V. N., Jayasurya, B., Bhavani, R., & Maiyalagan, T. (2024). Heterostructured FeSe2-CoSe2 nanorods supported on nitrogen and sulfur co-doped reduced graphene oxide as high-performance electrocatalyst for oxygen evolution reaction. *Journal of Alloys and Compounds*, *978*, 173313.

Jabeen, S., Veg, E., Ahmad, M. I., Bala, S., & Khan, T. (2025). A comprehensive review on metal oxide-based nanomaterials: synthesis, characterization, environmental, and therapeutic applications. *ChemistrySelect*, *10*(11), e202500080.

Sandhu, Z. A., Asifa, Shafqat, S. R., Danish, M., Batoo, K. M., Ijaz, M. F., ... & Ghaffar, S. (2025). Bi-functionality of hierarchical nano-granules like Co3O4 and CeO2-doped Co3O4 electrode materials for hydrogen evolution reaction and supercapacitor performance. *Ionics*, *31*(6), 6293-6308.

Xue, Z., Lv, L., Tian, Y., Tan, S., Ma, Q., Tao, K., & Han, L. (2021). Co3S4 nanoplate arrays decorated with oxygen-deficient CeO2 nanoparticles for supercapacitor applications. *ACS Applied Nano Materials*, *4*(3), 3033-3043.

Zhang, J., Wang, Y., Pan, L., Li, K., Zhang, J., Song, R., & Zhong, H. (2026). Cerium oxide-promoted cobalt sulfide prepared via cyclic voltammetry for enhanced hydrogen evolution reaction. *International Journal of Hydrogen Energy*, *231*, 154834.

Danish, M., Sandhu, Z. A., Sajid, S., Shafqat, S. R., Abbas, R., Shahid, M., ... & Raza, M. A. (2025). Role of engineered Co4S3 and Ce2S3-Co4S3 binary composite materials for clean and high-performance energy solutions. *Chalcogenide Lett.*, *22*(10), 863-870.

Kumar, S., Zhao, H., Haris, H. R., Sk, M., Lizhuang, D., Rashidi, M. M., ... & Thumu, U. (2026). Cu^{2+} as a dynamic director for Ce-incorporated $(CoFeNiCuCe)_9S_8$ nanoballs for multifunctional electrocatalysis. *Communications Chemistry*, *9*(1), 84.

Liu, R., Wang, C., Li, Y., Yan, Y., Yin, H., & Wu, T. (2026). Ultra low Co-doped CeO2 catalysts for enhanced toluene combustion: Unveiling structure-activity relationships and molecular oxygen activation capability. *Journal of Environmental Chemical Engineering*, *14*(5), 123511.

Dadi, D. G., Shura, M. W., & Gochole, F. (2025). DFT analysis of structural, electronic and optical properties of Ni and Zn doped CoS counter electrode for dye sensitized solar cells. *Scientific Reports*, *15*(1), 35486.

Grijalva-Saavedra, R., Suárez-Campos, G., Fuentes-Ríos, J., Ruiz-Molina, M., Solís-Mosquera, J., Quevedo-Lopez, M. A., ... & Sotelo-Lerma, M. (2025). Enhanced optical and electrical properties of Co-doped SnS thin films synthesized via chemical bath deposition. *Journal of Materials Science: Materials in Electronics*, *36*(1), 72.

Li, L., Zhou, J., Liu, D., Liu, X., Sun, Y., & Xiao, S. (2023). Performance and mechanism of co-doped Ce–Mn perovskite for degradation of tetracycline via heterogeneous photocatalysis coupled PMS oxidation. *Materials Science in Semiconductor Processing*, *154*, 107229.

Shen, C. H., Wen, X. J., Fei, Z. H., Liu, Z. T., & Mu, Q. M. (2020). Visible-light-driven activation of peroxymonosulfate for accelerating ciprofloxacin degradation using CeO2/Co3O4 pn heterojunction photocatalysts. *Chemical Engineering Journal*, *391*, 123612.

Wang, X., Li, W., Zhang, J., Zheng, J., Li, T., Du, C., ... & Xiong, C. (2025). Synergistic enhancement of tetracycline photodegradation in 5% Ce-doped Bi_2O_3–Co_3O_4/C: oxygen vacancy-mediated band engineering and singlet oxygen pathway optimization. *Journal of Environmental Chemical Engineering*, 120337.

Yang, F., Huang, Y., Fang, C., Xue, Y., Ai, L., Liu, J., & Wang, Z. (2018). Peroxymonosulfate/base process in saline wastewater treatment: the fight between alkalinity and chloride ions. *Chemosphere*, *199*, 84-88.

Gong, C., Chen, F., Yang, Q., Luo, K., Yao, F., Wang, S., ... & Zeng, G. (2017). Heterogeneous activation of peroxymonosulfate by Fe-Co layered doubled hydroxide for efficient catalytic degradation of Rhoadmine B. *Chemical engineering journal*, *321*, 222-232.

Zuo, X., Jiang, A., Zou, S., Wu, J., & Ding, B. (2023). Copper oxides activate peroxymonosulfate for degradation of methylene blue via radical and nonradical pathways: surface structure and mechanism. *Environmental Science and Pollution Research*, *30*(5), 13023-13038.

Mohanty, U. A., Sahoo, D. P., Das, K. K., Paramanik, L., & Parida, K. (2024). Facilitated visible-light-driven peroxymonosulfate activation by a Co–Fe layered double hydroxide derived p–n heterostructure for sulfadiazine degradation: affecting parameters, kinetics, and mechanistic insights. *Inorganic chemistry*, *63*(4), 1919-1937.

Zhang, R., Jin, Y., Xue, Z., Shao, J., Li, Q., & Yuan, N. (2026). Synergistic Mechanism of Peroxymonosulfate Activation and Photoexcitation on the Pyrolytic Bimetallic Metal–Organic Framework for Enhanced Charge Transfer. *ACS Applied Materials & Interfaces*, *18*(7), 11335-11348.

Lv, M., He, L., Zou, Z., Li, M., Hassan, M., & Gong, Z. (2025). Electronic structure and reactive species regulation by Co doping enhances MIL-100 (Fe) mediated photo-assisted PMS activation for ciprofloxacin degradation. *Applied Surface Science*, 165362.

Xie, M., Han, Y., Wang, N., Huang, Z., & Sun, C. (2025). Enhanced activation of PMS via Fe-MOFs-derives@ BC for efficient removal of dyes: Complementary between radical and nonradical pathways. *Journal of Water Process Engineering*, *77*, 108426.

Wang, N., Li, P., Wan, Y., Zhu, Z., Yan, Y., Yan, X., ... & Guo, Y. (2026). In-situ constructed NiCoFe-sulfide porous cube-like structure enable photo-synergistic PMS activation for efficient levofloxacin degradation. *Surfaces and Interfaces*, 109270.

Zhang, L., Zhao, X., Niu, C., Tang, N., Guo, H., Wen, X., ... & Zeng, G. (2019). Enhanced activation of peroxymonosulfate by magnetic Co3MnFeO6 nanoparticles for removal of carbamazepine: Efficiency, synergetic mechanism and stability. *Chemical Engineering Journal*, *362*, 851-864.

Tripathy, H., Binoy, T. R., Prajapati, S. C., & Kumar, A. (2026). Visible-Light-Driven $BiVO_4$-Alginate Hydrogel: An Ecofriendly High-Performance Photocatalyst for Tetracycline Hydrochloride Removal via Peroxymonosulphate Activation. *Water, Air, & SoilPollution*, *237*(15), 878.

Anipsitakis GP, Dionysiou DD. Degradation of organic contaminants in water with sulfate radicals generated by the conjunction of peroxymonosulfate with cobalt. *Environmental Science & Technology*. 2003;37(20):4790–4797.

Azaizeh M, et al. Photocatalytic mechanisms for peroxymonosulfate activation through the removal of methylene blue: a case study. *International Journal of Environmental Research and Public Health*. 2019;16(2):198.

Oh WD, Dong Z, Lim TT. Generation of sulfate radical through heterogeneous catalysis for organic contaminants removal: current development, challenges and prospects. *Applied Catalysis B: Environmental*. 2016;194:169–185.

Wang, H., Chen, H., Wan, Q., Zheng, Y., Wan, Y., Liu, X., ... & Huo, P. (2025). Catalytic degradation of polyethylene terephthalate microplastics by Co-N/C@ CeO2 composite in thermal-assisted activation PMS system: process mechanism and toxicological analysis. *Chemical Engineering Journal*, *514*, 163192.

Akmal, A., Tahir, D., Heryanto, H., Artasasta, M. A., & Musa, B. (2025). Fundamentals of electrocatalysis and photocatalysis for the remediation of wastewater containing methylene blue. *Environmental Science and Pollution Research*, *32*(31), 18604-18630.

Xie, M., Han, Y., Wang, N., Huang, Z., & Sun, C. (2025). Enhanced activation of PMS via Fe-MOFs-derives@ BC for efficient removal of dyes: Complementary between radical and nonradical pathways. *Journal of Water Process Engineering*, *77*, 108426.